17. Magnetic Energy Release

Magnetic Energy Release

1. Solar Energetic Phenomena
2. Energy Equation
3. Two Types of Magnetic Energy Release
4. Rapid Dissipation: Sweet's Mechanism
5. Petschek's Mechanism
6. Numerical Models of Magnetic Reconnection
7. Observations of Magnetic Reconnection

Solar Energetic Phenomena

The energy accumulated in solar magnetic fields is often released in powerful explosive events, such as flares and coronal mass ejections (CME). Most of the energy is released in the form of heat, high-speed motions, UV and X-ray radiation and energetic particles.

The total energy emitted in explosive events in the solar atmosphere may exceed 10^{32} erg or 10^{25} J. Most explosive events occur in active regions.

Observations of emerging magnetic flux and magnetic energy release in EUV from TRACE satellite

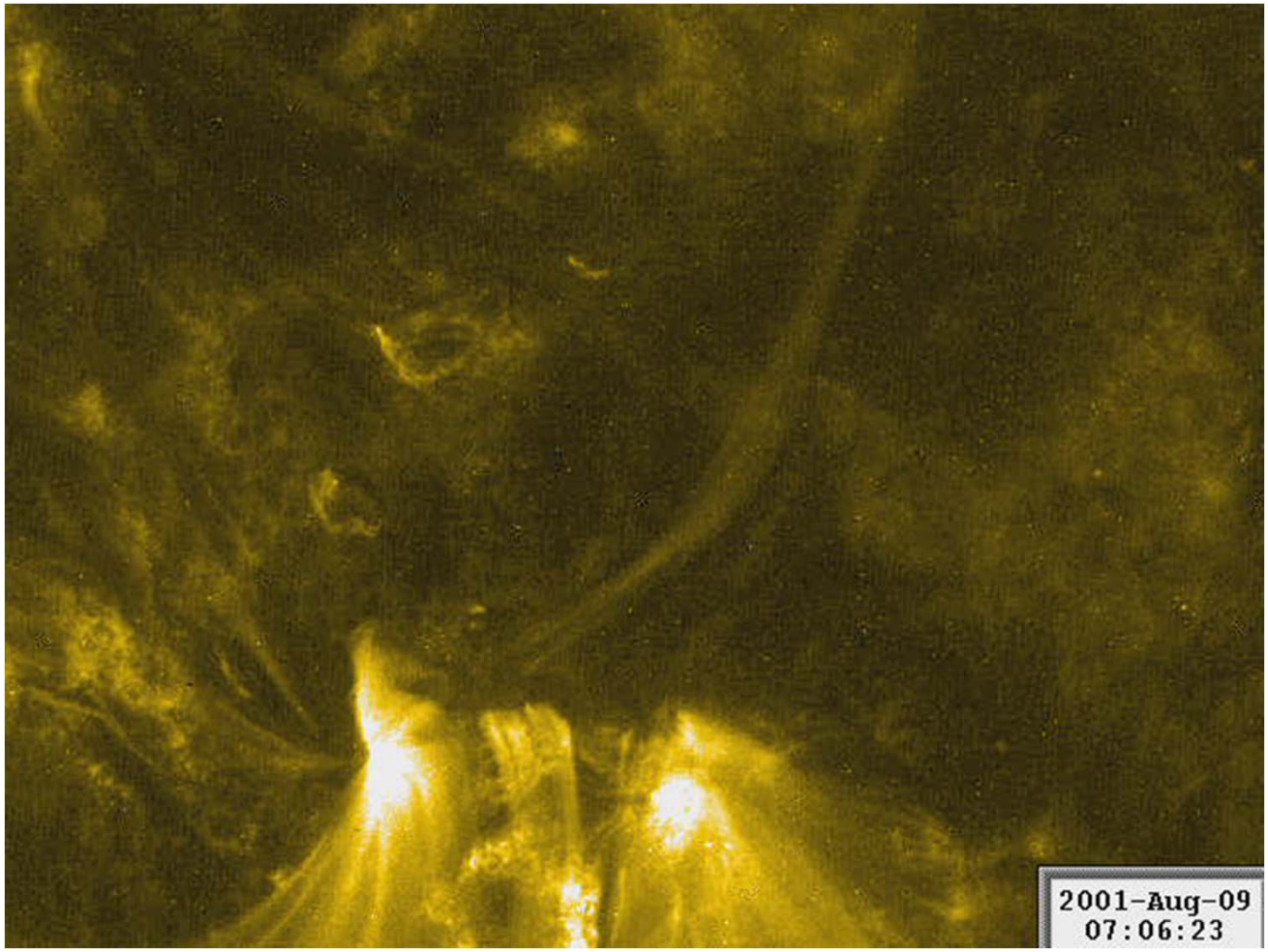

Energy Equation

We use the general MHD equations to obtain an energy balance equation that contains all the different types of energy, including kinetic energy due to plasma motions, the internal energy due to the gas pressure and the magnetic energy.

We will perform the following steps:

1. Consider the full system of MHD equations
2. Derive an equation for the kinetic energy
3. Derive an equation for the sum of the kinetic and magnetic energy
4. Consider the magnetic energy balance and discuss the Poynting flux
5. Derive an equation for the total energy density: internal+kinetic+magnetic.

MHD equations

Consider the system of MHD equation:

$$\frac{\partial \rho}{\partial t} + \nabla(\rho \mathbf{v}) = 0, \quad \text{- continuity equation (conservation of mass)}$$

$$\rho \frac{d\mathbf{v}}{dt} = \rho\left[\frac{\partial \mathbf{v}}{\partial t} + (\mathbf{v}\nabla)\mathbf{v}\right] = -\nabla P + \frac{1}{c}\mathbf{j}\times\mathbf{B}, \text{ - momentum equation}$$

$$\rho\left[\frac{dE}{dt} + P\frac{d}{dt}\left(\frac{1}{\rho}\right)\right] = Q - L, \quad \text{- energy equation}$$

$$\frac{\partial \mathbf{B}}{\partial t} = \nabla\times(\mathbf{v}\times\mathbf{B}) - \frac{c^2}{4\pi}\nabla\times\left(\frac{1}{\sigma}\nabla\times\mathbf{B}\right), \text{ - induction equation}$$

$$\mathbf{j} = \sigma\left(\mathbf{E} + \frac{1}{c}\mathbf{v}\times\mathbf{B}\right), \text{ - Ohm's law}$$

where $E = \dfrac{P}{(\gamma-1)\rho}$ is the internal energy density; Q is the heating rate (e.g. Joule heating), and L is the cooling energy rate (e.g. due to radiation).

Example: For a fully ionized hydrogen plasma: $\rho = Mn_p$, where M is the proton mass, $n_p = n_e = n$ is the number of protons and electrons in a unit volume; $\gamma=5/3$; $P=(n_p+n_e)kT$; $E=3/2(n_p+n_e)kT/(Mn_p)$
We get $E=3(k/M)T=3/2RT/\mu$; $P=R\rho T/\mu$; $R=k/M$ is the gas constant; $\mu=0.5$ is the molecular weight.

Equation for kinetic energy

First, we multiply the momentum equation:

$$\rho \frac{d\mathbf{v}}{dt} = -\nabla P + \frac{1}{c}\mathbf{j}\times\mathbf{B},$$

by $\mathbf{v}$ to obtain an equation for the kinetic plasma energy $E_K = \rho\mathbf{v}^2/2$:

$$\frac{d}{dt}\left(\frac{\rho\mathbf{v}^2}{2}\right) = -\mathbf{v}\nabla P + \frac{1}{c}\mathbf{v}(\mathbf{j}\times\mathbf{B}).$$

This equation shows that the kinetic energy of a plasma element changes due to the work of the pressure force $-\nabla P$ and the Lorentz force $\frac{1}{c}\boldsymbol{v}\times\boldsymbol{B}$.

Transformation of the Lorentz force work term $\frac{1}{c}\mathbf{v}(\mathbf{j}\times\mathbf{B})$

Using the triple product relation: $\mathbf{a}(\mathbf{b}\times\mathbf{c}) = -\mathbf{b}(\mathbf{a}\times\mathbf{c})$ and the Ohm's law:

$$\frac{1}{c}\mathbf{v}\times\mathbf{B} = \frac{\mathbf{j}}{\sigma} - \mathbf{E},$$

we obtain $$\frac{1}{c}\mathbf{v}(\mathbf{j}\times\mathbf{B}) = -\frac{1}{c}\mathbf{j}(\mathbf{v}\times\mathbf{B}) = \mathbf{j}\cdot\mathbf{E} - \frac{j^2}{\sigma}.$$

Using the Maxwell equations: $\mathbf{j} = \frac{c}{4\pi}\nabla\times\mathbf{B}$, and $\nabla\times\mathbf{E} = -\frac{1}{c}\frac{\partial\mathbf{B}}{\partial t}$,

we calculate the dot product:

$$\mathbf{j}\cdot\mathbf{E} = \frac{c}{4\pi}(\nabla\times\mathbf{B})\mathbf{E} = -\frac{c}{4\pi}\nabla(\mathbf{E}\times\mathbf{B}) + \frac{c}{4\pi}\mathbf{B}\cdot\nabla\times\mathbf{E} =$$

$$= -\frac{c}{4\pi}\nabla(\mathbf{E}\times\mathbf{B}) - \frac{1}{8\pi}\frac{\partial\mathbf{B}^2}{\partial t}.$$

Here we used the vector formula: $\nabla(\mathbf{E}\times\mathbf{B}) = \mathbf{E}\cdot\nabla\times\mathbf{B} + \mathbf{B}\cdot\nabla\times\mathbf{E}.$

Equation for the sum of kinetic and magnetic energy

Substituting these relations into the kinetic energy equation one gets:

$$\frac{d}{dt}\left(\frac{\rho \mathbf{v}^2}{2}\right) = -\mathbf{v}\nabla P - \frac{\mathbf{j}^2}{\sigma} - \frac{c}{4\pi}\nabla(\mathbf{E}\times\mathbf{B}) - \frac{1}{8\pi}\frac{\partial \mathbf{B}^2}{\partial t},$$

finally,

$$\frac{\partial}{\partial t}\left(\frac{\rho \mathbf{v}^2}{2} + \frac{\mathbf{B}^2}{8\pi}\right) + \nabla\left(\frac{\rho \mathbf{v}^2}{2}\mathbf{v} + c\frac{\mathbf{E}\times\mathbf{B}}{4\pi}\right) = -\mathbf{v}\nabla P - \frac{\mathbf{j}^2}{\sigma}.$$

Here $\frac{\mathbf{B}^2}{8\pi}$ is the magnetic energy density,

$c\frac{\mathbf{E}\times\mathbf{B}}{4\pi}$ is the Poynting flux, $\frac{\mathbf{j}^2}{\sigma}$ is the Joule dissipation.

This equation shows that the total kinetic and magnetic energy of plasma at a given position (Eulerian coordinates!) can change due to the work of pressure force, $-\mathbf{v}\nabla P$, and the Joule dissipation, also due to the energy flux: $\frac{\rho \mathbf{v}^2}{2}\mathbf{v} + c\frac{\mathbf{E}\times\mathbf{B}}{4\pi}$.

Example: The Poynting Flux and Coronal Heating (B.Welsch)

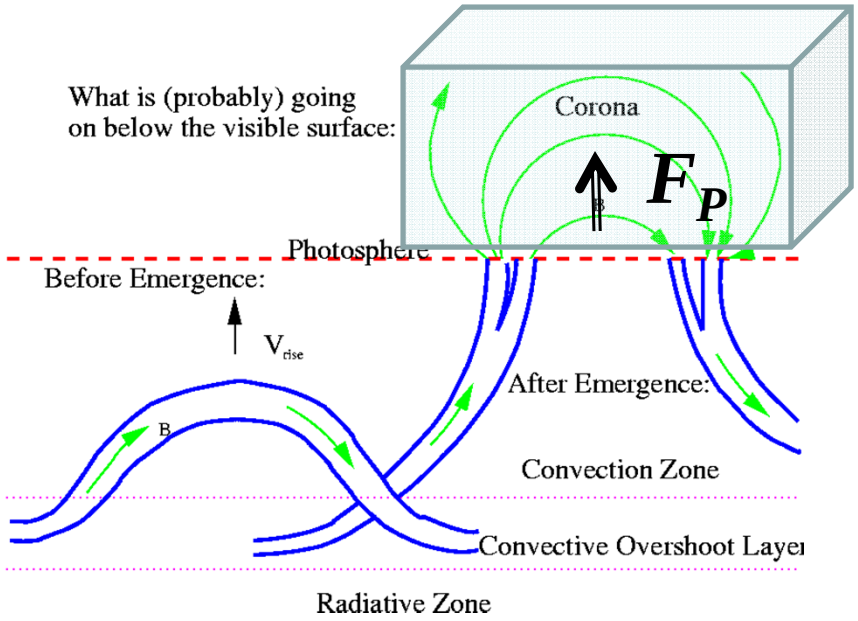

The magnetic energy balance:

$$\frac{\partial}{\partial t}\left(\frac{\mathbf{B}^2}{8\pi}\right)+\nabla\left(c\frac{\mathbf{E}\times\mathbf{B}}{4\pi}\right)=-\frac{\mathbf{j}^2}{\sigma}.$$

Assume the ideal MHD approximation $(\sigma=\infty)$ and integrate this equation over a volume in the atmosphere with the bottom boundary in the photosphere and apply the Gauss theorem:

$$\frac{\partial}{\partial t}\int_V\left(\frac{\mathbf{B}^2}{8\pi}\right)dV=\int_S \boldsymbol{F}_P d\boldsymbol{s},\ \text{where}\ \boldsymbol{F}_P=c\frac{\mathbf{E}\times\mathbf{B}}{4\pi}\ \text{is the Poynting flux.}$$

$\boldsymbol{E}$ can be calculated from the Omh's law: $\boldsymbol{j}=\sigma(\boldsymbol{E}+\frac{1}{c}\boldsymbol{v}\times\boldsymbol{B})$; for $\sigma=\infty$: $\boldsymbol{E}=-\frac{1}{c}\boldsymbol{v}\times\boldsymbol{B}$.

Then $\boldsymbol{F}_P=-(\boldsymbol{v}\times\boldsymbol{B})\times\mathbf{B}/4\pi$ can be calculated from photospheric measurements of $\boldsymbol{v}$ and $\boldsymbol{B}$.

It was found that the average $\boldsymbol{F}_P$ is sufficient to explain coronal heating, with values near $(5\pm1)\times10^7$ erg cm^{-2} s^{-1}. The energy flux required for coronal heating ~ 10^7 erg cm^{-2}s^{-1}, for chromospheric heating: 2×10^7 erg cm^{-2} s^{-1} (Welsch, 2015, *Publ. Astr.Soc.Jap.* 67 (2), 18).

Equation for the total energy density

Consider the internal energy equation. Using the mass conservation equation the energy equation can be written as

$$\rho \frac{dE}{dt} + P\nabla \mathbf{v} = Q - L,$$

or by combining it with the continuity equation: $\frac{\partial \rho}{\partial t} + \nabla(\rho \mathbf{v}) = 0,$

we obtain: $$\frac{\partial}{\partial t}(\rho E) + \nabla\left(\frac{\gamma}{\gamma - 1} P\mathbf{v}\right) = -\mathbf{v}\nabla P + Q - L.$$

Finally, by adding this equation to the equation for the kinetic and magnetic energy we get ***the equation for the total energy density***

$$\frac{\partial}{\partial t}\left(\rho E + \frac{\rho \mathbf{v}^2}{2} + \frac{\mathbf{B}^2}{8\pi}\right) + \nabla\left(\frac{\rho \mathbf{v}^2}{2}\mathbf{v} + \frac{\gamma}{\gamma - 1} P\mathbf{v} + c\frac{\mathbf{E} \times \mathbf{B}}{4\pi}\right) = Q - \frac{\mathbf{j}^2}{\sigma} - L.$$

kinetic energy flux enthalpy flux Poynting flux

The total energy is conserved (changed only due to radiative losses) if

$$Q = \frac{\mathbf{j}^2}{\sigma}.$$ This is the Joule heating formula.

Dissipation of magnetic energy

The magnetic energy density is $\mathbf{B}^2/8\pi$; it dissipates in the form of Joule heating. Only non-potential field ($\mathbf{j} \neq 0$) can dissipate (release energy).

The non-potential portion of magnetic energy is called free energy.

Consider magnetic energy stored in the form of non-potential field of $B = 100$ G in a volume of 10^{27} cm^3 (10x10x10 Mm^3) - typical coronal conditions:

$$E_M = \frac{B^2 L^3}{8\pi} = 4 \times 10^{29} \text{ erg.}$$

This is comparable but less than the energy release in large flares. Therefore, a stronger field in larger volumes has to dissipate.

Two Types of Magnetic Energy Release

We can distinguish between "non-explosive" and "explosive" energy release.

Any non-potential field carries electric current and dissipates gradually due to Joule heating. This is non-explosive release.

Estimate the non-explosive dissipation time: $t_J \sim \frac{B^2/8\pi}{j^2/\sigma}$,

where $j \sim \frac{c}{4\pi}\frac{B}{L}$, and L is a characteristic size.

Then, $t_J \sim \frac{2\pi\sigma L^2}{c^2}$ is similar to the magnetic diffusion time

$$t_{diff} \sim \frac{4\pi\sigma L^2}{c^2}.$$

The factor of 2 difference is insignificant in this estimates.

Comparison of Joule dissipation and dynamic characteristic times

Introducing the **coefficient of magnetic diffusivity** $\eta = \dfrac{c^2}{4\pi\sigma}$

we can write $t_J \sim \dfrac{L^2}{\eta}.$

In the solar photosphere and chromosphere $\eta \simeq 10^7$ cm^2/s, in the corona - $\eta \simeq 3\times 10^3$ cm^2/s.

Compare this with a typical dynamic time: $t_d \sim \dfrac{L}{v}$:

$$t_J = \frac{L^2}{\eta} = \frac{Lv}{\eta}\frac{L}{v} = R_M t_D,$$

where $R_M = \dfrac{Lv}{\eta} = \dfrac{4\pi\sigma Lv}{c^2} = \dfrac{4\pi\sigma L^2}{c^2 t_D}$

is the magnetic Reynolds number for a dynamic process with scale L and characteristic time t_D .

Characteristic time of non-explosive dissipation

If $R_M >> 1$ then $t_J >> t_D$, and magnetic dissipation is not significant for the dynamic process.

Consider a dynamic process with **Alfven speed** (e.g. waves, shock, high-speed flows) $c_A = \dfrac{B}{\sqrt{4\pi\rho}} \sim 10^8$ cm/s.

Then, $t_J = \dfrac{L^2}{\eta} = \dfrac{Lc_A}{\eta}\dfrac{L}{c_A} = N_L \dfrac{L}{c_A} = N_L t_A,$

where $N_L = \dfrac{Lc_A}{\eta}$ is the **Lundquist number**,

$t_A = L/c_A$ is the **Alfven wave crossing time**.

Therefore, the characteristic time of non-explosive dissipation for dynamic processes with a characteristic Alfven speed is $t_J = \dfrac{LN_L}{c_A}$.

Characteristic time of explosive dissipation

$N_L = \dfrac{Lc_A}{\eta}$ is the **Lundquist number**,

$t_A = L/c_A$ is the **Alfven wave crossing time**.

$t_J = \dfrac{LN_L}{c_A}$ is the **Joule dissipation time**.

For the coronal conditions in solar flares:

$L \sim 10^9$ cm, $c_A \sim 10^8$ cm/s, $\eta \simeq 3\times 10^3$ cm^2/s: $N_L \sim 10^{17}/10^3 \sim 10^{14}$,

the crossing time $L/c_A \sim 10$ sec. Then, $t_J \sim 10^{15}$ sec.

For a mechanism of rapid dissipation (Sweet-Parker) we'll see that the Lundquist number has a power 1/2: $t_R \sim \dfrac{LN_L^{1/2}}{c_A}$.

For flare conditions $t_R \sim 10^8$ sec, this is still too long.

For Petchek's mechanism of explosive dissipation: $t_P \sim \dfrac{L \ln N_L}{c_A}$,

that is about 300 sec. This is close to flare times.

Magnetic dissipation in current sheets

Dissipation of magnetic fields occurs mostly in very thin layers carrying electric current ("current sheets"). These are formed by plasma motions. Photospheric turbulence continuously deforms magnetic fields and increases free energy. Strong local deformations $\Delta\mathbf{B}$ produce current sheets.

Rapid dissipation occurs only where the topology of magnetic field provide Maxwell stresses in a form to drive the current sheets towards vanishing thickness.

It was realized that explosive dissipation must occur around singular places in magnetic field (such as neutral points $B = 0$ where dissipation can occur despite the small resistivity.

Example: formation of thin current sheets due to winding of magnetic field lines by photospheric motions (Parker)

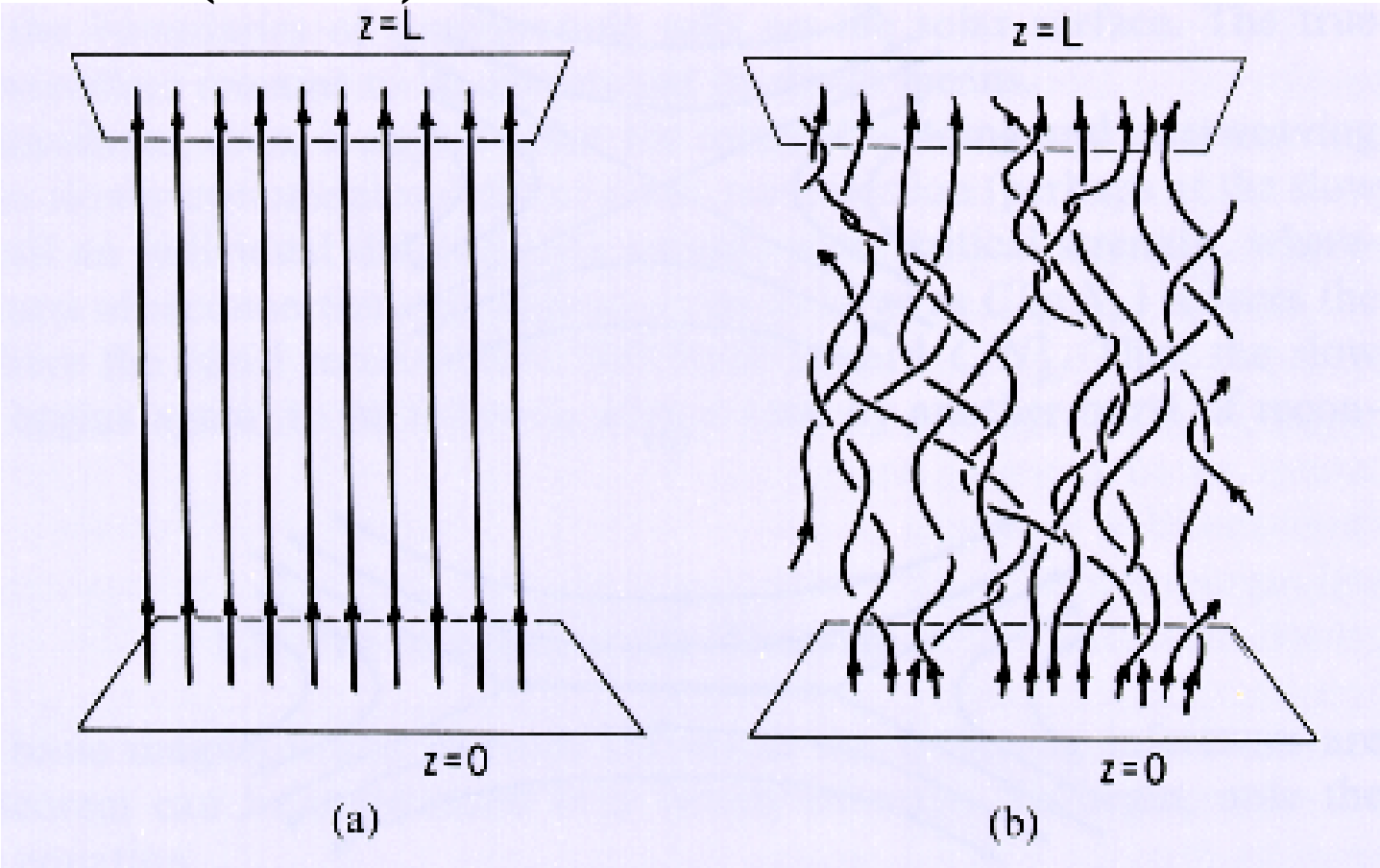

A sketch of the arbitrary winding of the field lines due to photospheric motions.

2D Reconnection

David Pontin

University of St Andrews

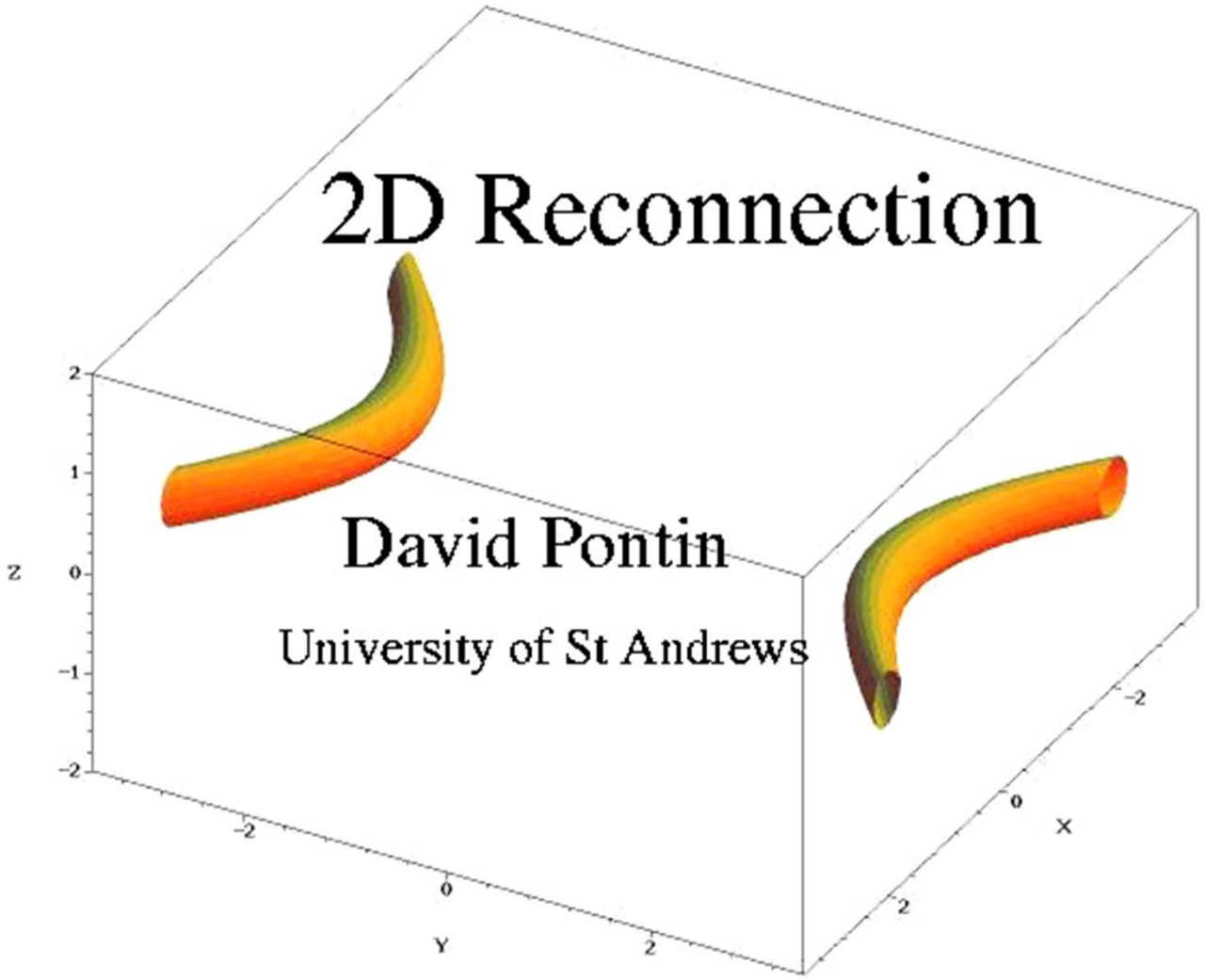

Rapid Dissipation: Sweet-Parker Mechanism

Sweet (1956) considered two antiparallel fields pressed together over length l . The fluid is squeezed out between two parallel fields, causing the field gradient steepen until the resistive dissipation creates a steady state.

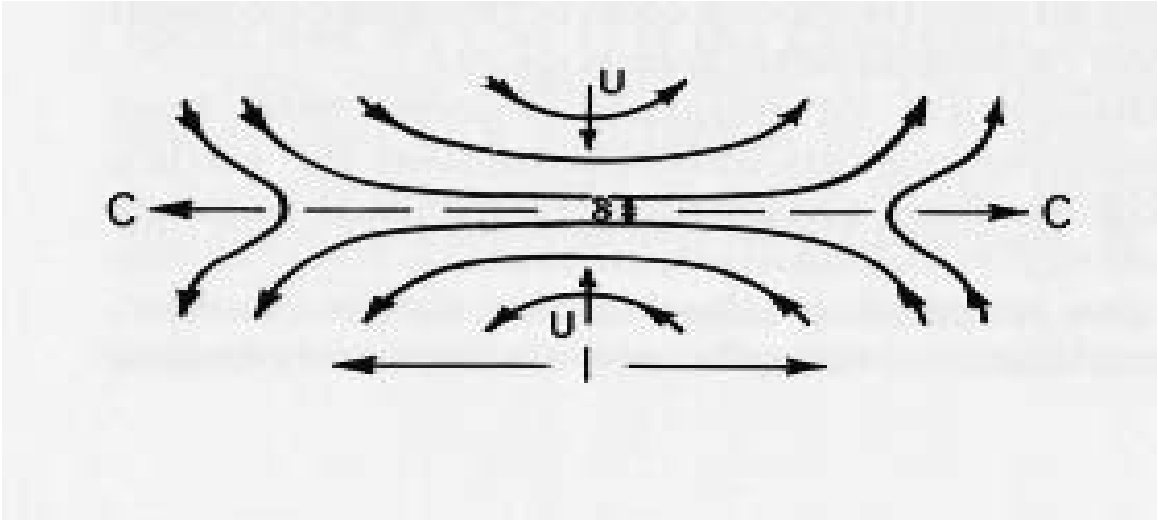

A schematic drawing of the field lines undergoing rapid reconnection across the dashed center line.

Calculation of the characteristic reconnection time (Parker, 1957)

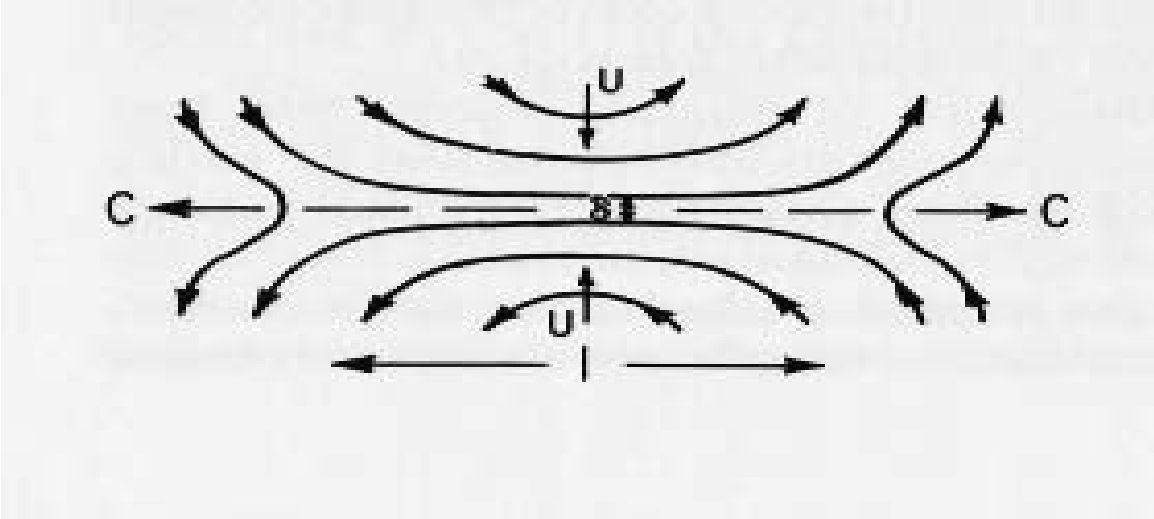

Mass balance: $UL = C\delta,$

where $U = \eta/\delta$ - diffusion time, $C = c_A$ - characteristic outflow speed.

then, $\delta = \sqrt{\frac{L\eta}{c_A}},$ $U = \frac{\eta}{\delta} = \sqrt{\frac{c_A\eta}{L}} = \frac{c_A}{N_L^{1/2}},$

where $N_L = c_A L/\eta$. This is the reconnection speed.

Therefore, the characteristic reconnection time:

$$t_S = \frac{L}{U} = \frac{LN_L^{1/2}}{c_A}.$$

Petschek's Mechanism

Petschek (1964) suggested that two opposite fields $\pm B$ of scale l may, as a consequence of the dynamics of the inflow and outflow, come into contact across a narrow width h which is much smaller than the full width l .
Sonnerup (1970) argued that the rate of reconnection can be as small as desired by pushing the opposite fields firmly together.

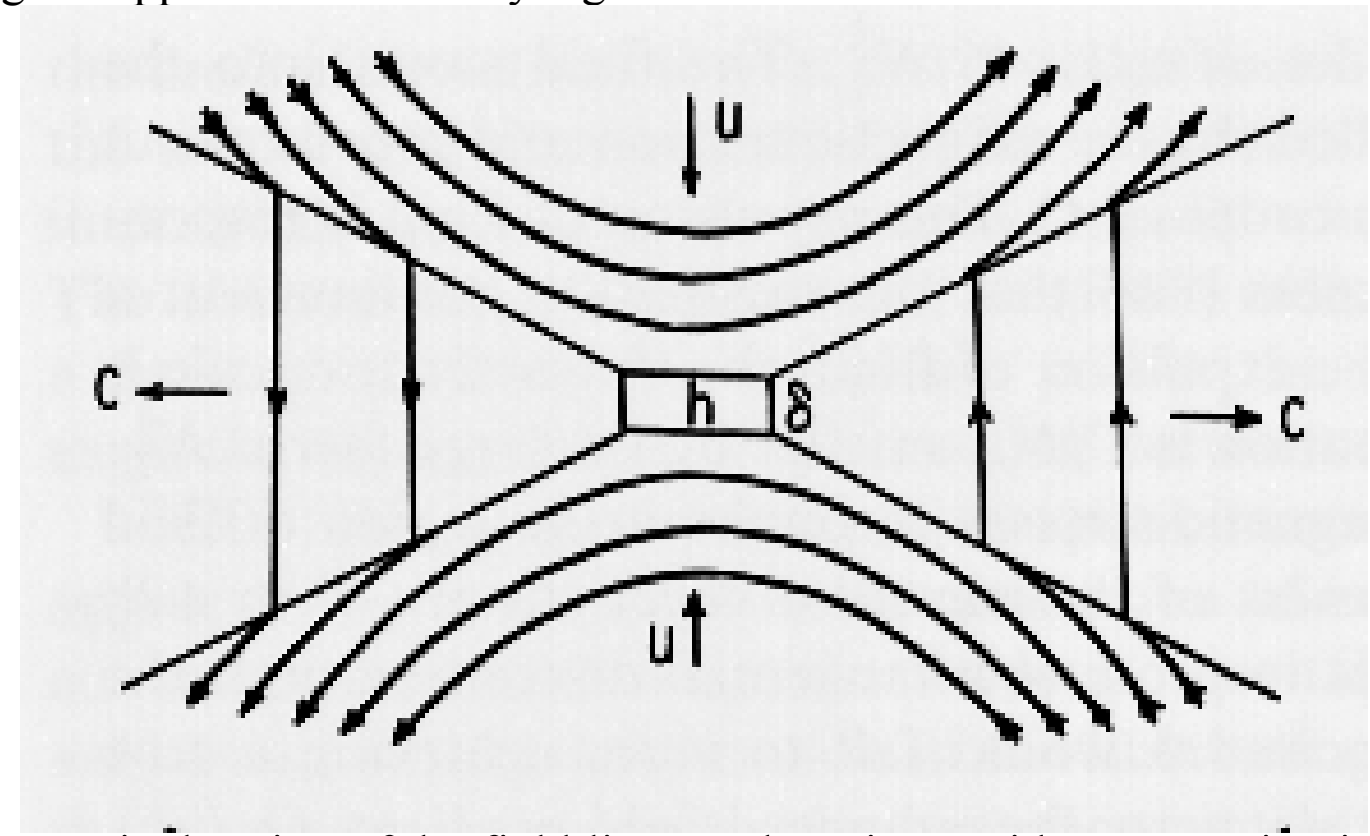

A schematic drawing of the field lines undergoing rapid reconnection in Petschek's model.

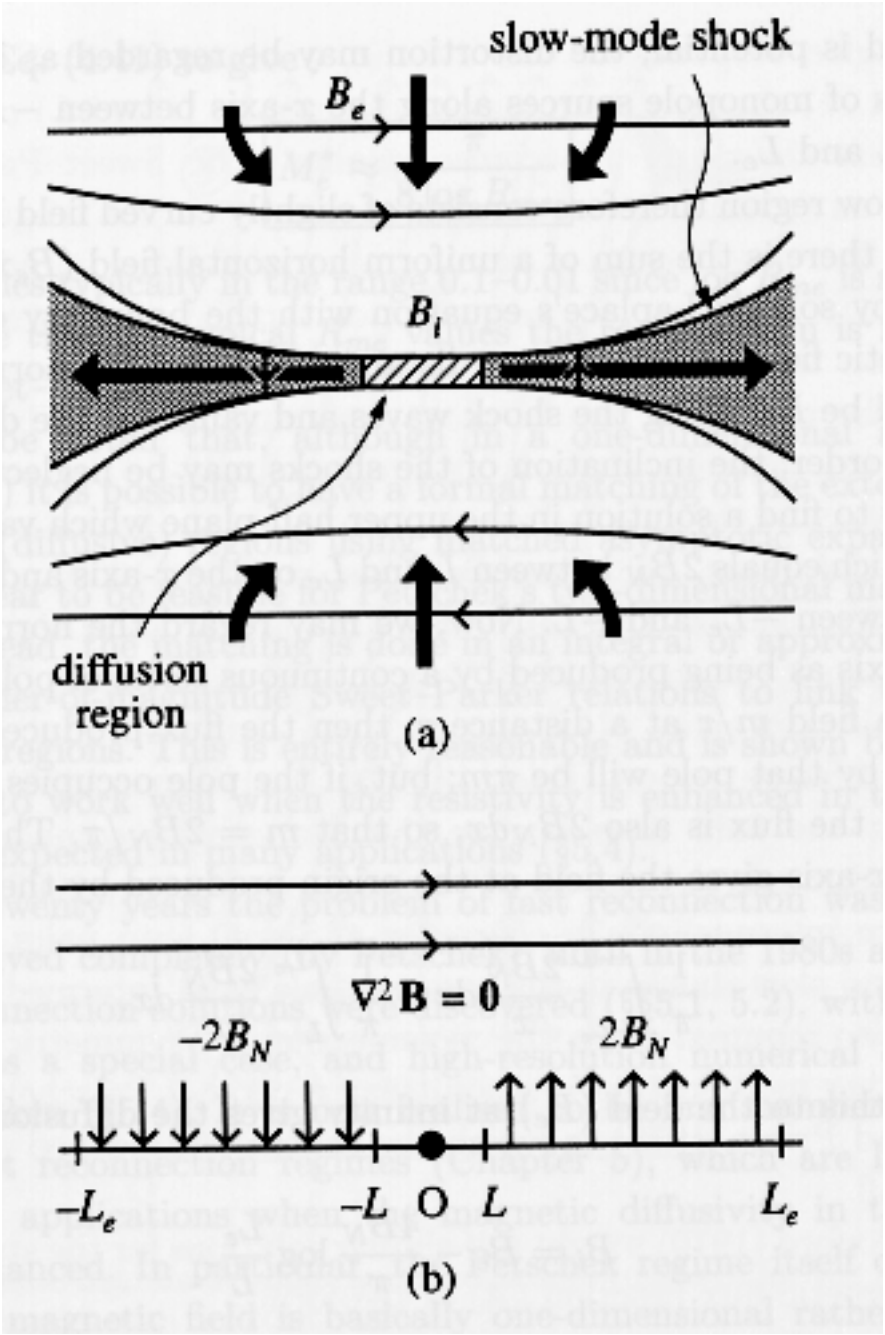

Petschek's model, in which the central shaded region is the diffusion region and the other two shaded regions represent plasma that is heated and accelerated by the shocks.

In Petschek's model a slow magnetoacoustic shock provides another way (in addition to a diffusion region) of converting magnetic energy into heat and kinetic energy.

Physical Interpretation of Petschek's Solution (Semenov)

temporarily enhanced “anomalous” resistivity

Anomalous resistivity may occur as a result of plasma instabilities in regions of high electric current density when the speed of electrons reaches the speed of plasma waves, or due to small-scale turbulence.

Anomalous resistivity may significantly decrease the dissipation time.

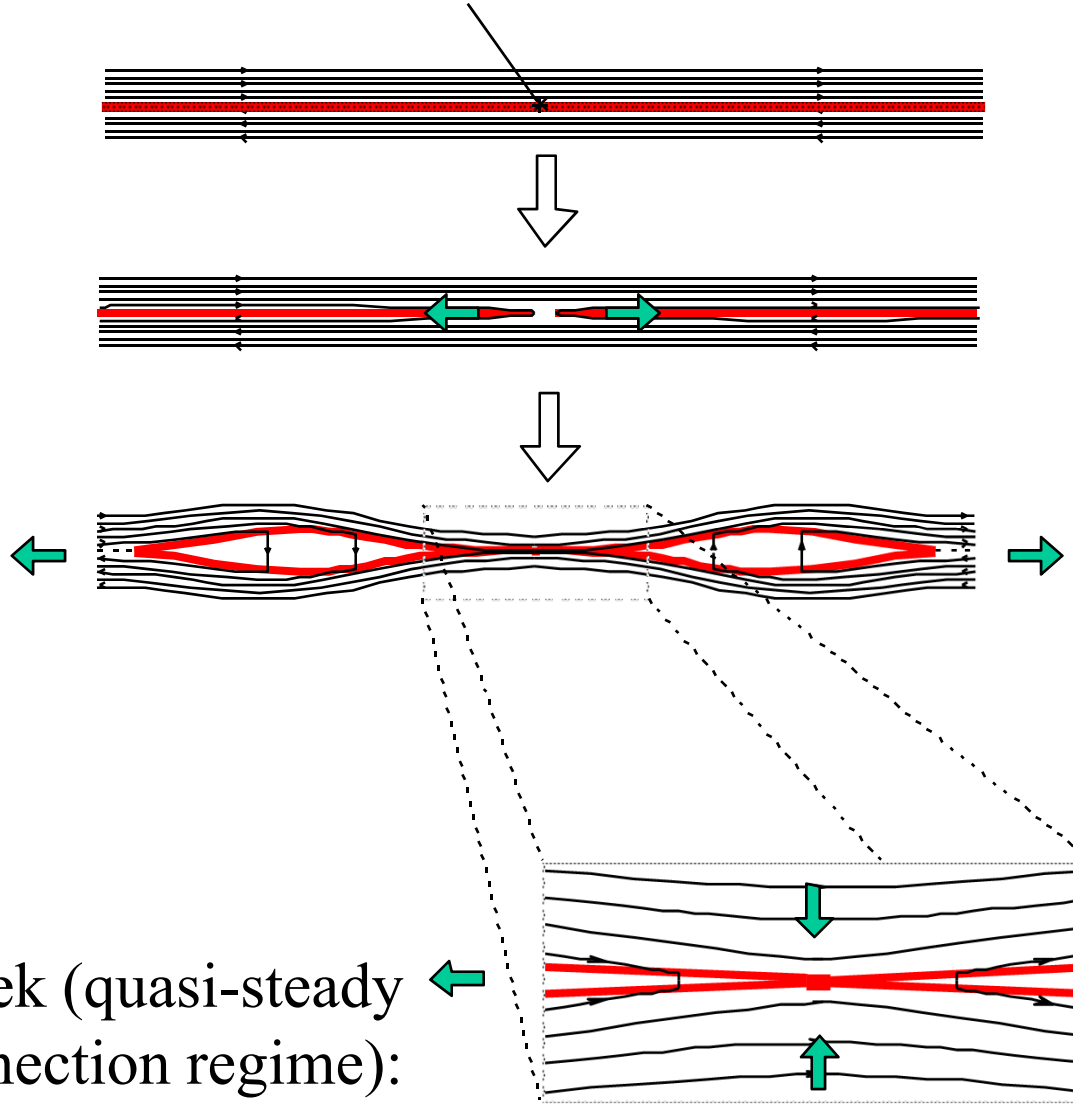

Petschek (quasi-steady Reconnection regime):

Numerical Models of Magnetic Reconnection

Takaaki Yokoyama and Kazunari Shibata, 2001, Magnetohydrodynamic Simulation of a Solar Flare with Chromospheric Evaporation Effect Based on the Magnetic Reconnection Model, The Astrophysical Journal, 549:1160-1174, 2001.

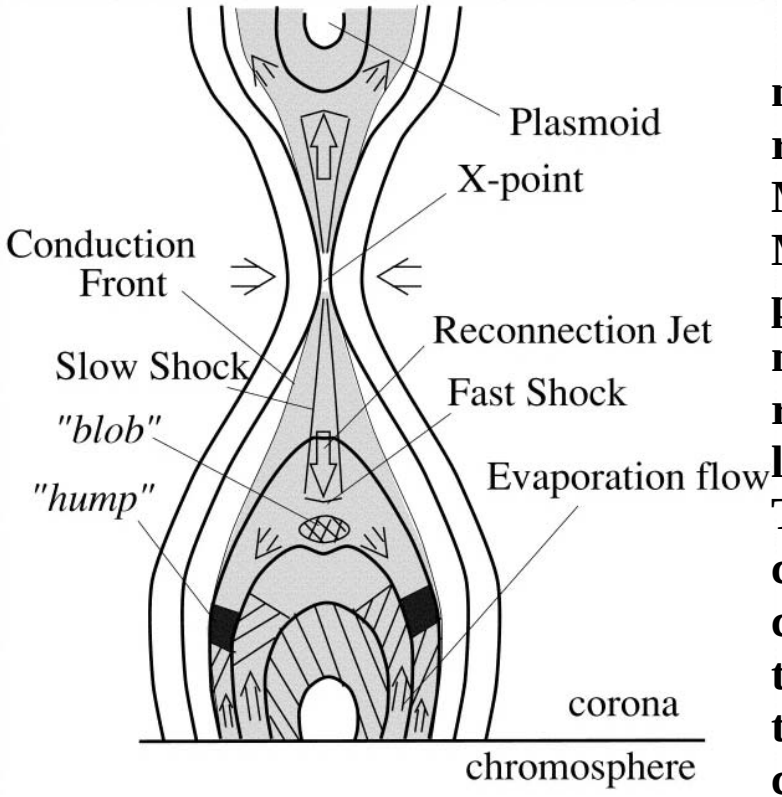

Schematic illustration of the reconnection model of a solar flare based on the simulation results. Thick solid lines show magnetic field. Magnetic energy is released at slow-mode MHD shocks emanating from the neutral X-point, which is formed as a result of the magnetic reconnection. The ejected reconnection jet collides with the reconnected loops and forms a fast-mode MHD shock. The released heat at the reconnection site conducts along the field lines down to the chromosphere. Because of the heat input into the dense chromospheric plasma, the plasma there evaporates and flows back toward the corona.

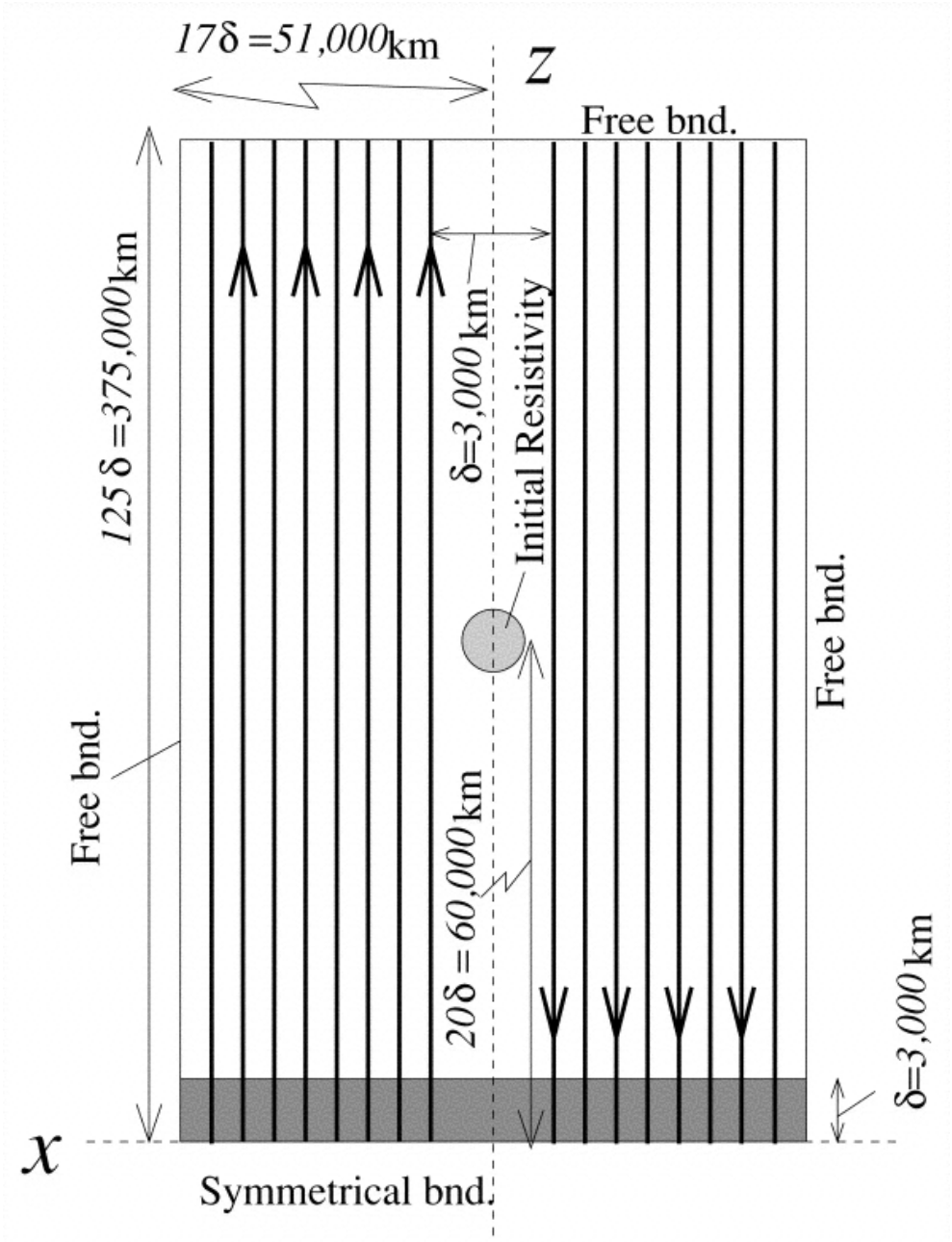

Initial condition of the simulation.

Lines with arrows are magnetic field lines. The hatched circle is the region where initial resistivity perturbation is imposed. The hatched region near z = 0 is the chromosphere.

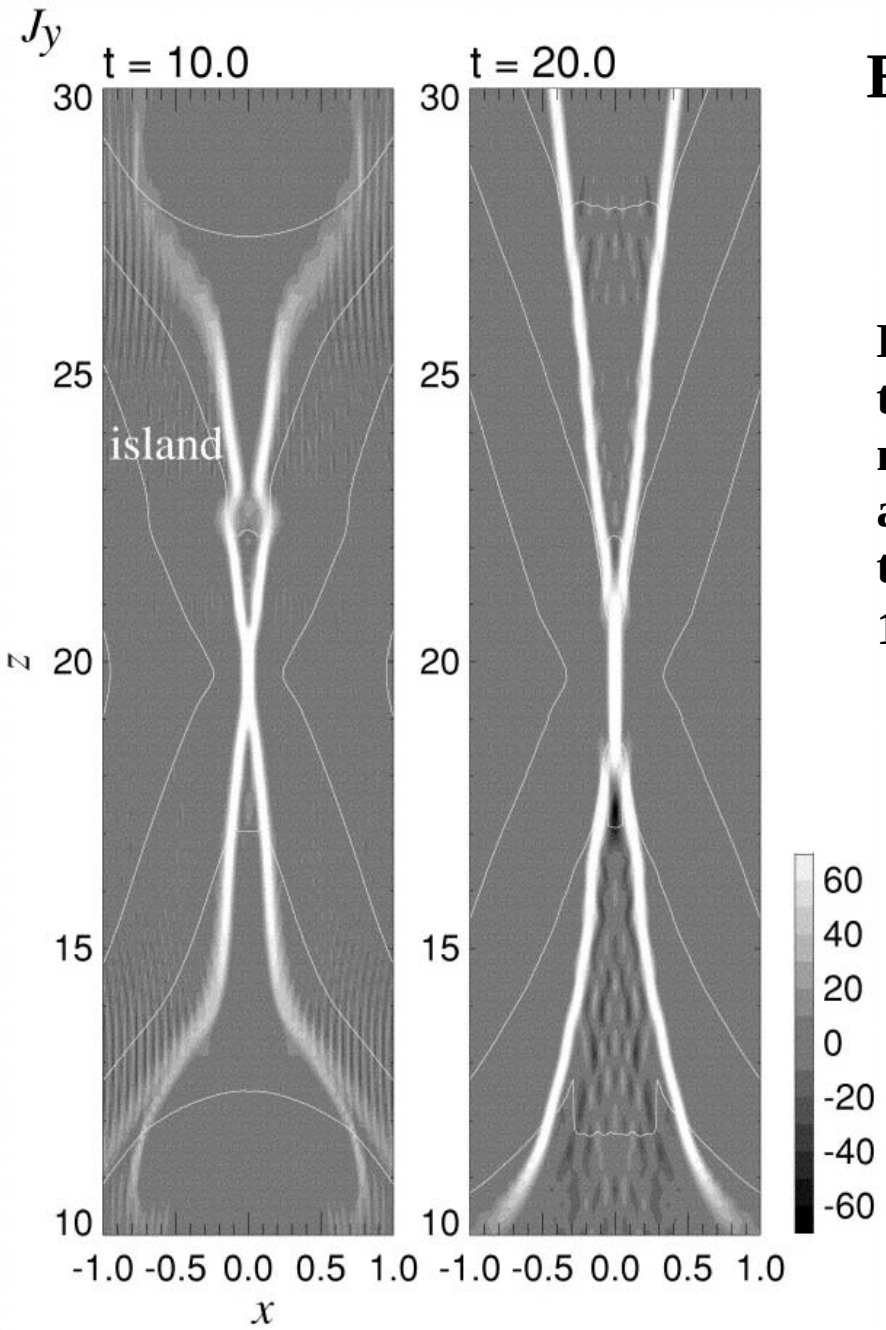

Electric current density

Evolution of two-dimensional plot of the y-component of the current density near the X-point. The X-point is located at (x,z) = (0, 20). The units of length, time, and current density are 3000 km, 18 s, and 4×10^{3} cgs, respectively.

Evolution of plasma temperature and density

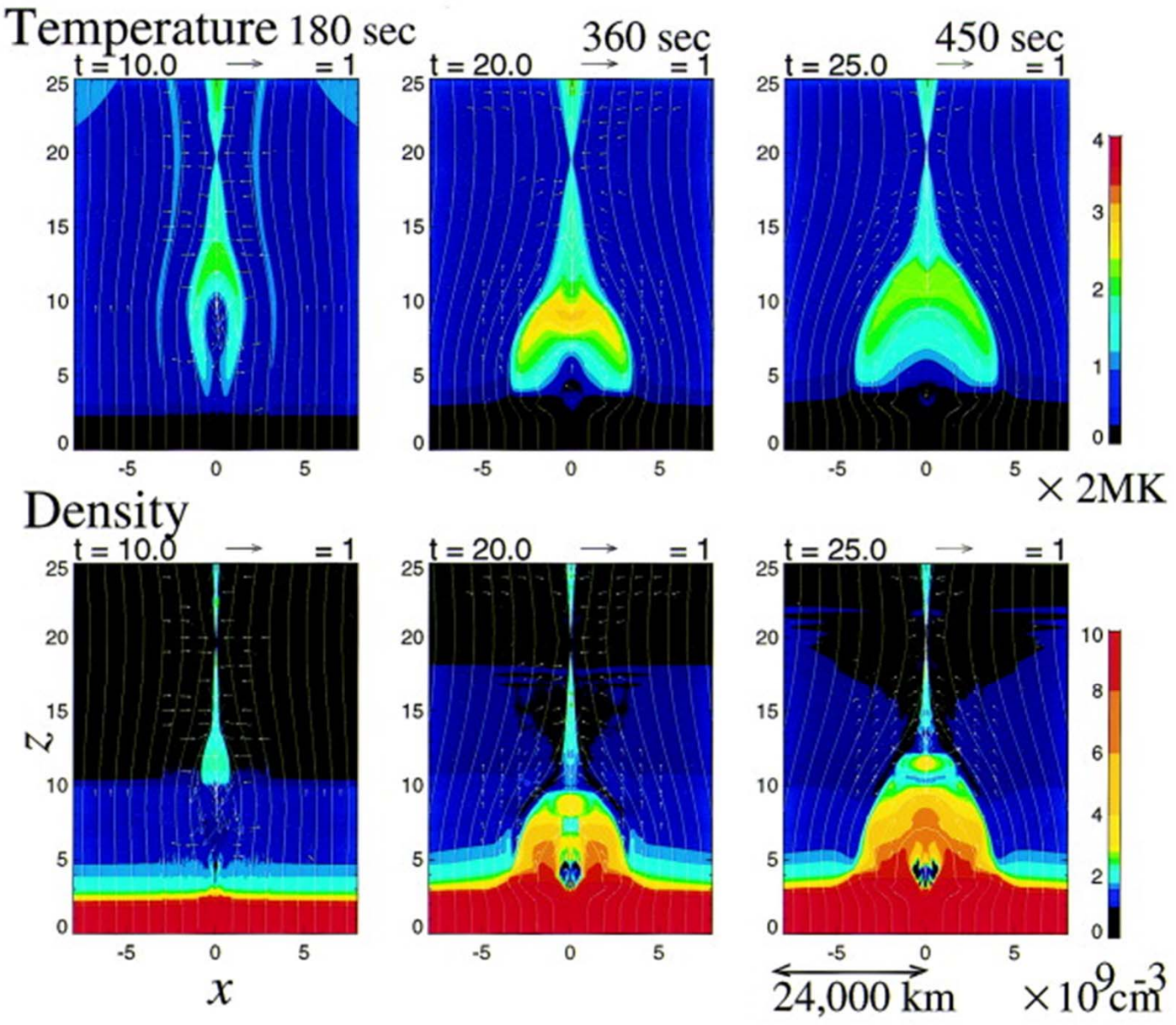

Observational evidence for magnetic reconnection – plasma heating at the top of magnetic loops

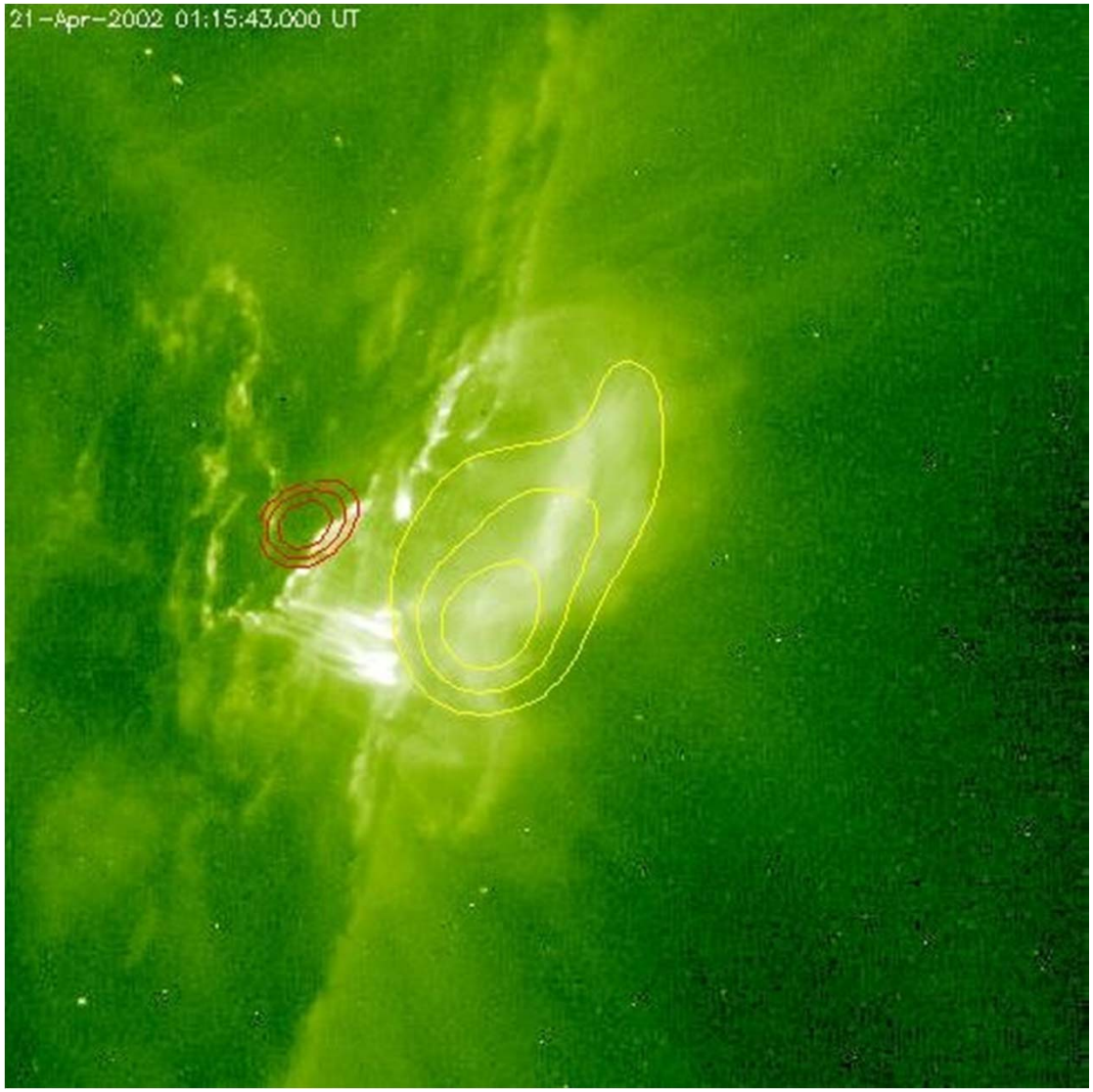

Gallagher et al., Solar Phys. 2002

X-ray sources during the 2002/08/24 X3.1 flare

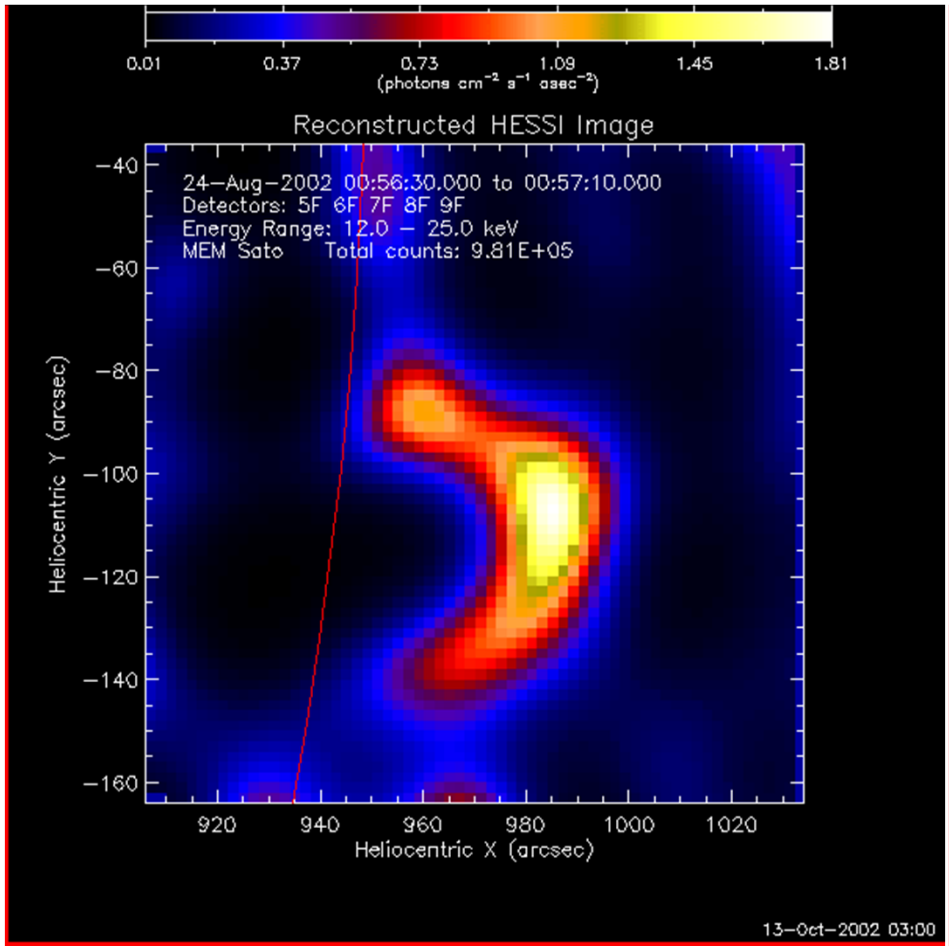

12 - 25 keV

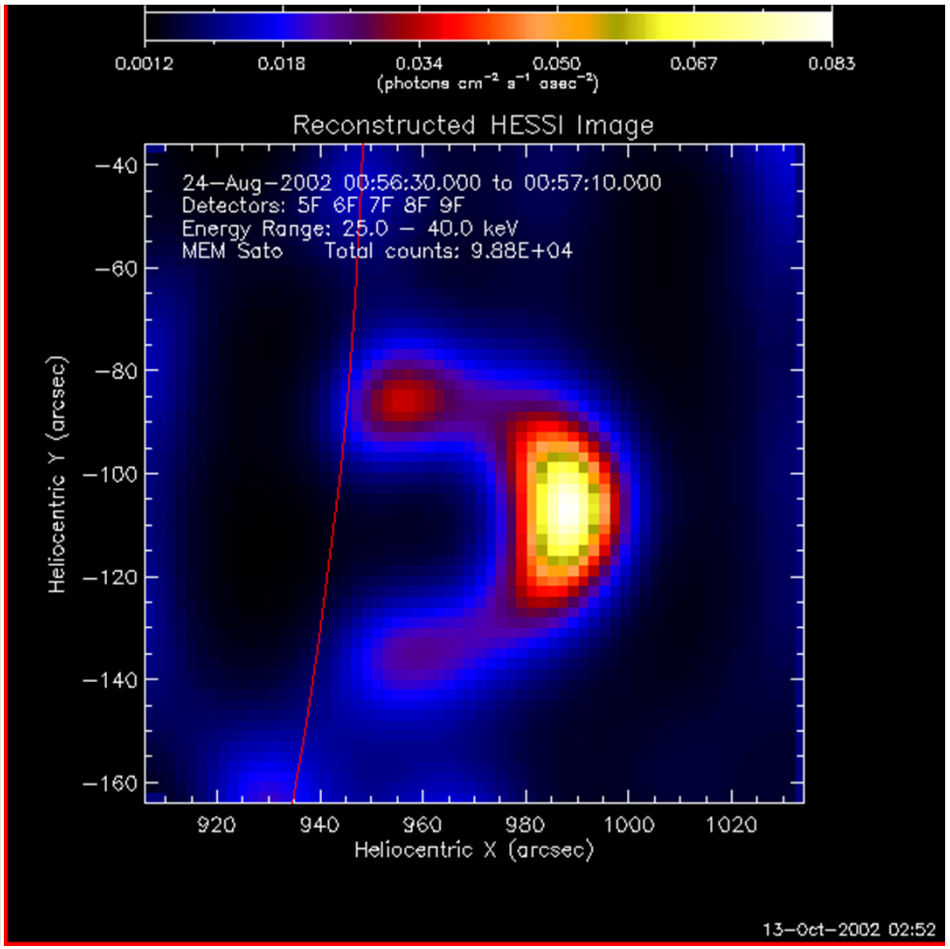

25 - 40 keV

Observations of Magnetic Reconnection

Aschwanden et al, 1999, Quadrupolar Magnetic Reconnection in Solar Flares. I. Three-dimensional Geometry Inferred from Yohkoh Observations, The Astrophysical Journal, 526:1026-1045.

They analyzed the three-dimensional geometry of solar flares that show so-called interacting flare loops in soft X-ray. The two flare loops that appear brightest after the flare are assumed to represent the outcome of a quadrupolar magnetic reconnection process, during which the connectivity of magnetic polarities is exchanged between the four loop footpoints. The authors parameterized the three-dimensional geometry of the four involved magnetic field lines with circular segments, additionally constrained by the geometric condition that the two pre-reconnection field lines have to intersect each other at the onset of the reconnection process, leading to a 10 parameter model. They fit this 10 parameter model to Yohkoh Soft and Hard X-Ray Telescopes (SXT and HXT) data of 10 solar flares and determine in this way the loop sizes and relative orientation of interacting field lines before and after reconnection.

Geometrical model of magnetic loops

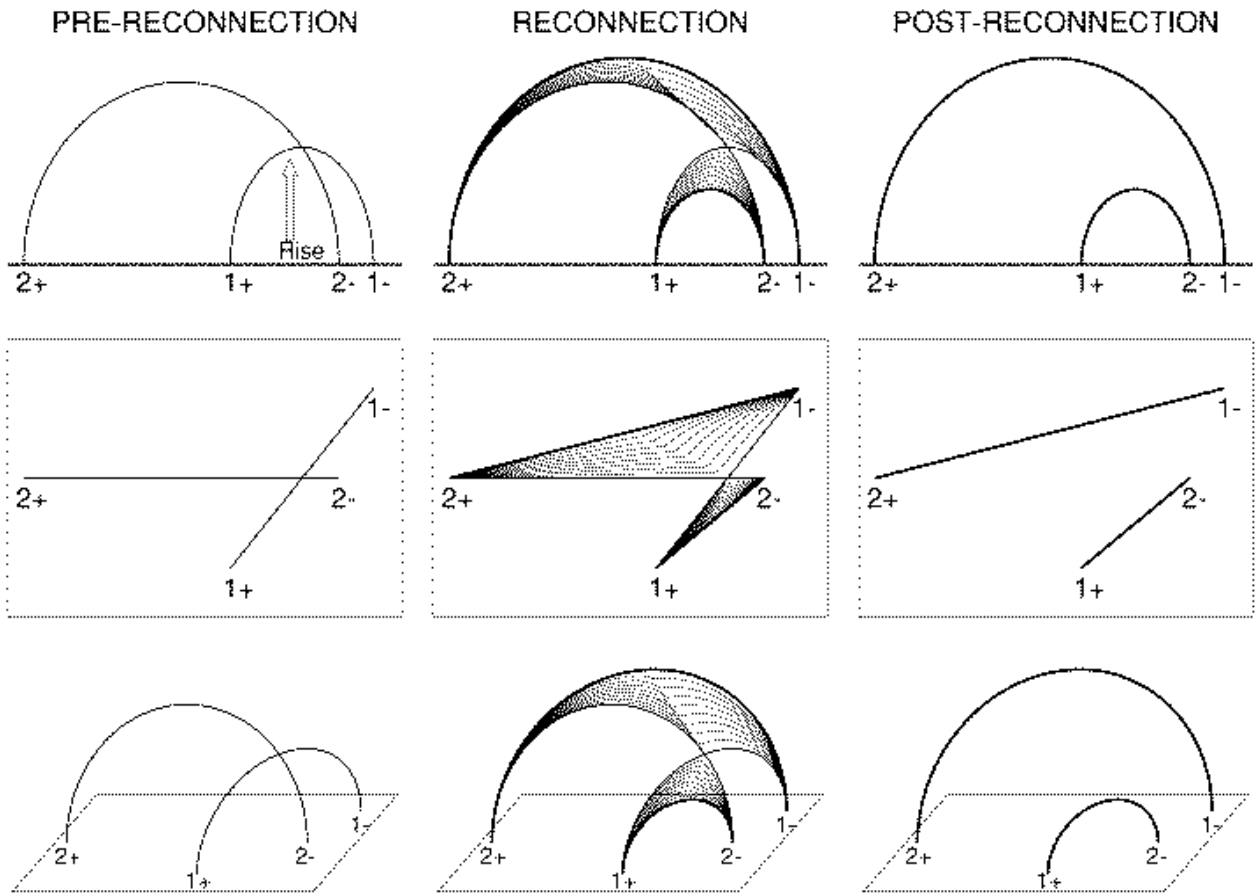

The three-dimensional geometry of the four involved magnetic field lines with circular segments, additionally constrained by the geometric condition that the two pre-reconnection field lines have to intersect each other at the onset of the reconnection process, leading to a 10 parameter model. They fit this 10 parameter model to Yohkoh Soft and Hard X-Ray Telescopes (SXT and HXT) data of 10 solar flares and determine in this way the loop sizes and relative orientation of interacting field lines before and after reconnection.

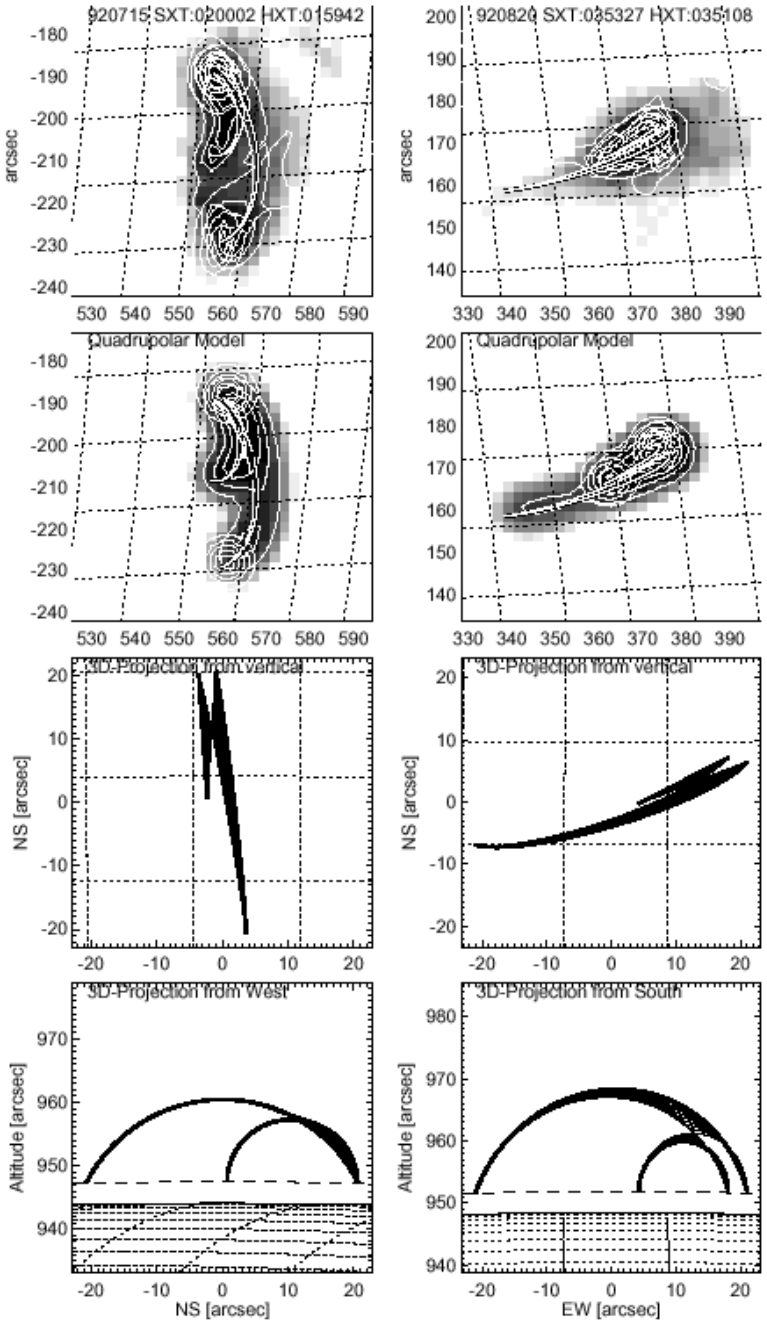

Fitting the model to X-ray images of magnetic loops

Top row in each set: Soft X-ray image (logarithmic gray scale and thin contours) from Yohkoh/SXT and hard X-ray image (thick contours) from Yohkoh/HXT. The thin circular segments represent the geometric solutions of the pre-reconnection field lines, and the thick circular segments show the corresponding post-reconnection field lines, which coincide with the flare loops.

Second row: Simulated SXR and HXR maps constrained by the three-dimensional quadrupolar model, represented with identical gray scales and contour levels as the original data (top row).

Third row: Geometric solution of the three-dimensional quadrupolar model rotated so that the vertical z-axis coincides with the line of sight. Ten field lines are interpolated between the pre- and post-reconnection state, visualizing the relaxation process of field lines after reconnection.

Bottom row: Same three-dimensional model rotated so that either the x-axis (viewed from west) or the y-axis (viewed from south) coincides with the line of sight. The spacing of the heliographic grid is 1 degree (corresponding to 12,150 km) in all frames.

The findings and conclusions are the following:

1. The pre-reconnection field lines always show a strong asymmetry in size, consistent with the scenario of newly emerging small-scale loops that reconnect with preexisting large-scale loops.
2. The relative angle between reconnecting field lines is nearly collinear in half of the cases, and nearly perpendicular in the other half, contrary to the antiparallel configuration that is considered to be most efficient for magnetic reconnection.
3. The angle between interacting field lines is reduced by 10-50 deg after quadrupolar reconnection.
4. The small-scale flare loop experiences a shrinkage by a factor of 1.31 ± 0.44, which is consistent with the scaling law found from previous electron time-of-flight measurements, suggesting that electron acceleration occurs near the cusp of quadrupolar configurations.

Recent development – models and observations of “slipping” reconnection: the footpoints of reconnecting magnetic lines “slip” along the flare ribbons of a “J-shape” that is formed by a overlying flux rope (Javier, et al, 2014, ApJ, 788:60, 1)

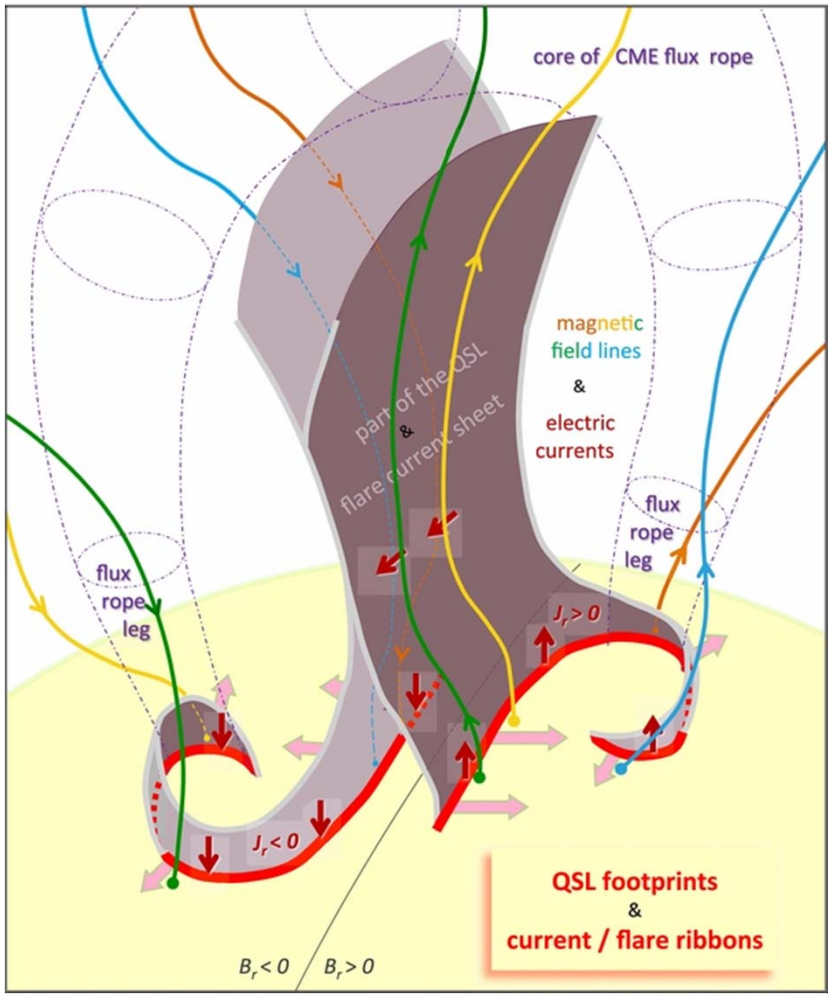

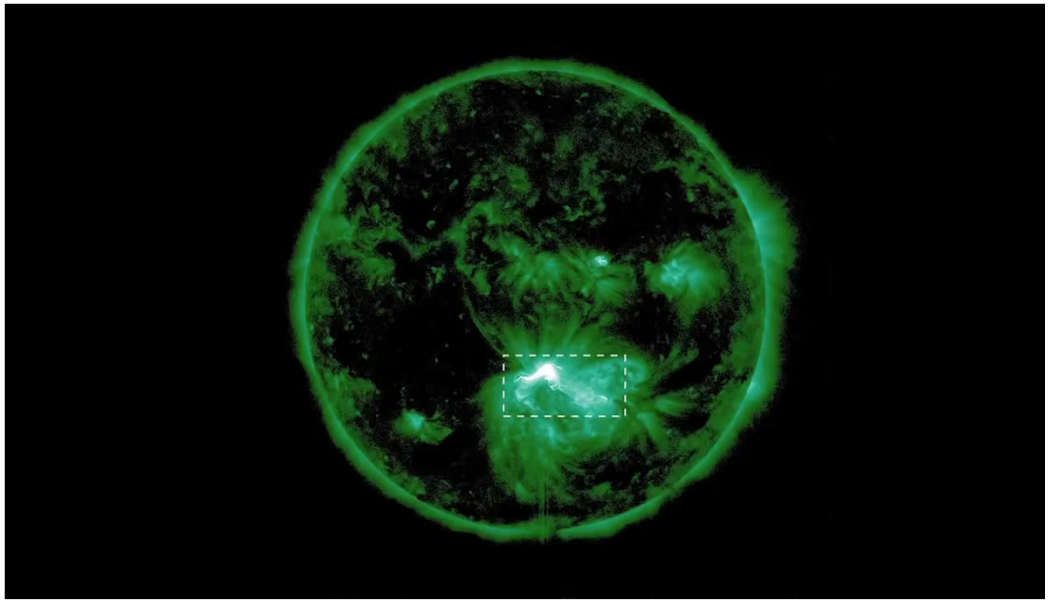

Reconnection experiments - MRX

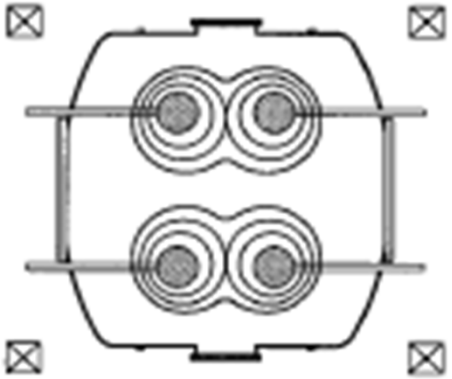

- Magnetic Reconnection eXperiment (Princeton) $T_e \approx$ 50,000 - 300,000 K,

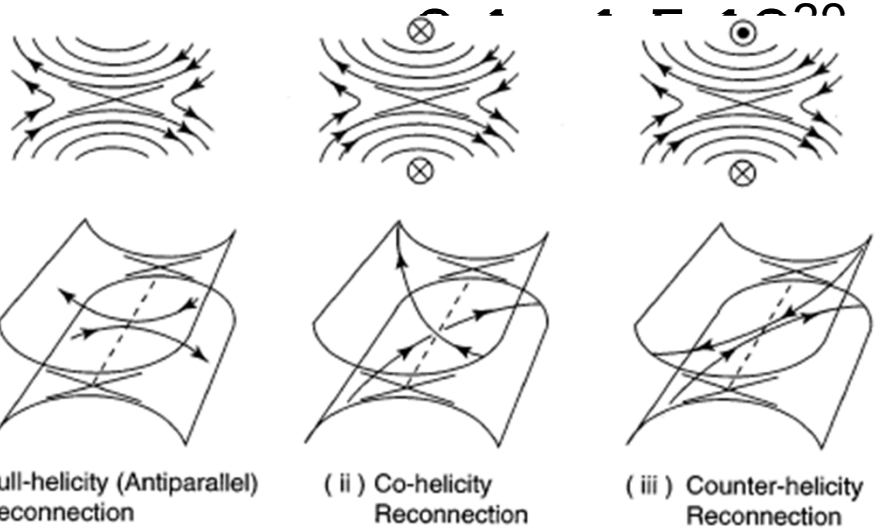

Yamada et al, 1997, Ji et al, 2001)...